Phase formation in the (1-y)$BiFeO_3$-y$BiScO_3$ system under ambient and high pressure

A.N. Salak, D.D. Khalyavin, A.V. Pushkarev, Yu.V. Radyush, N.M. Olekhnovich, A.D. Shilin, V.V. Rubanik

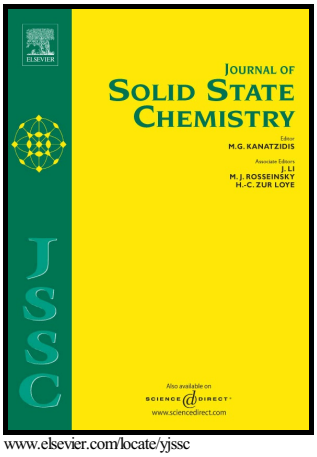

www.elsevier.com/locate/yjssc

PII: S0022-4596(16)30512-6
DOI: http://dx.doi.org/10.1016/j.jssc.2016.12.029
Reference: YJSSC19648

To appear in: *Journal of Solid State Chemistry*

Received date: 4 November 2016
Revised date: 30 December 2016
Accepted date: 31 December 2016

Cite this article as: A.N. Salak, D.D. Khalyavin, A.V. Pushkarev, Yu.V. Radyush, N.M. Olekhnovich, A.D. Shilin and V.V. Rubanik, Phase formation in the (1-y)$BiFeO_3$-y$BiScO_3$ system under ambient and high pressure, *Journal of Solid State Chemistry,* http://dx.doi.org/10.1016/j.jssc.2016.12.029

Phase formation in the (1-*y*)$BiFeO_3$-*y*$BiScO_3$ system under ambient and high pressure

A.N. Salak[1*], D.D. Khalyavin[2#], A.V. Pushkarev[3], Yu.V. Radyush[3], N.M. Olekhnovich[3], A.D. Shilin[4], V.V. Rubanik[4]

[1]*Department of Materials and Ceramic Engineering and CICECO – Aveiro Institute of Materials, University of Aveiro, 3810-193 Aveiro, Portugal*

[2]*ISIS Facility, Rutherford Appleton Laboratory, Chilton, OX11 0QX Didcot, UK*

[3]*Scientific-Practical Materials Research Centre of NAS of Belarus, P. Brovka Street, 19, 220072 Minsk, Belarus*

[4]*Institute of Technical Acoustics of NAS of Belarus, Lyudnikov Avenue, 13, 210023 Vitebsk, Belarus*

[*] salak@ua.pt

[#] dmitry.khalyavin@stfc.ac.uk

Abstract

Formation and thermal stability of perovskite phases in the $BiFe_{1-y}Sc_yO_3$ system ($0 \le y \le 0.70$) were studied. When the iron-to-scandium substitution rate does not exceed about 15 at.%, the single-phase perovskite ceramics with the rhombohedral *R*3*c* symmetry (as that of the parent compound, $BiFeO_3$) can be prepared from the stoichiometric mixture of the respective oxides at ambient pressure. Thermal treatment of the oxide mixtures with a higher content of scandium results in formation of two main phases, namely a $BiFeO_3$-like *R*3*c* phase and a cubic (*I*23) sillenite-type phase based on γ-Bi_2O_3. Single-phase perovskite ceramics of the $BiFe_{1-y}Sc_yO_3$ composition were synthesized under high pressure from the thermally treated oxide mixtures. When *y* is between 0 and 0.25 the high-pressure prepared phase is the rhombohedral *R*3*c* with the $\sqrt{2}a_p \times \sqrt{2}a_p \times 2\sqrt{3}a_p$ superstructure ($a_p \sim 4$ Å is the pseudocubic perovskite unit-cell parameter). The orthorhombic *Pnma* phase ($\sqrt{2}a_p \times 4a_p \times 2\sqrt{2}a_p$) was obtained in the range of $0.30 \le y \le 0.60$, while the monoclinic *C*2/*c* phase ($\sqrt{6}a_p \times \sqrt{2}a_p \times \sqrt{6}a_p$) is formed when $y=0.70$. The normalized unit-cell volume drops at the crossover from the rhombohedral to the orthorhombic composition range. The perovskite $BiFe_{1-y}Sc_yO_3$ phases prepared under high pressure are metastable regardless of their symmetry. At ambient pressure, the phases with the compositions in the ranges of $0.20 \le y \le 0.25$, $0.30 \le y < 0.50$ and $0.50 \le y \le 0.70$ start to decompose above 970, 920 and 870 K, respectively.

Graphical Abstract

Formation of perovskite phases in the $BiFe_{1-y}Sc_yO_3$ system when $y \geq 0.15$ requires application of pressure of several GPa. The phases formed under high pressure: *R*3*c* ($y \leq 0.25$), *Pnma* ($0.30 \leq y \leq 0.60$) and *C*2/*c* ($y \geq 0.70$) are metastable.

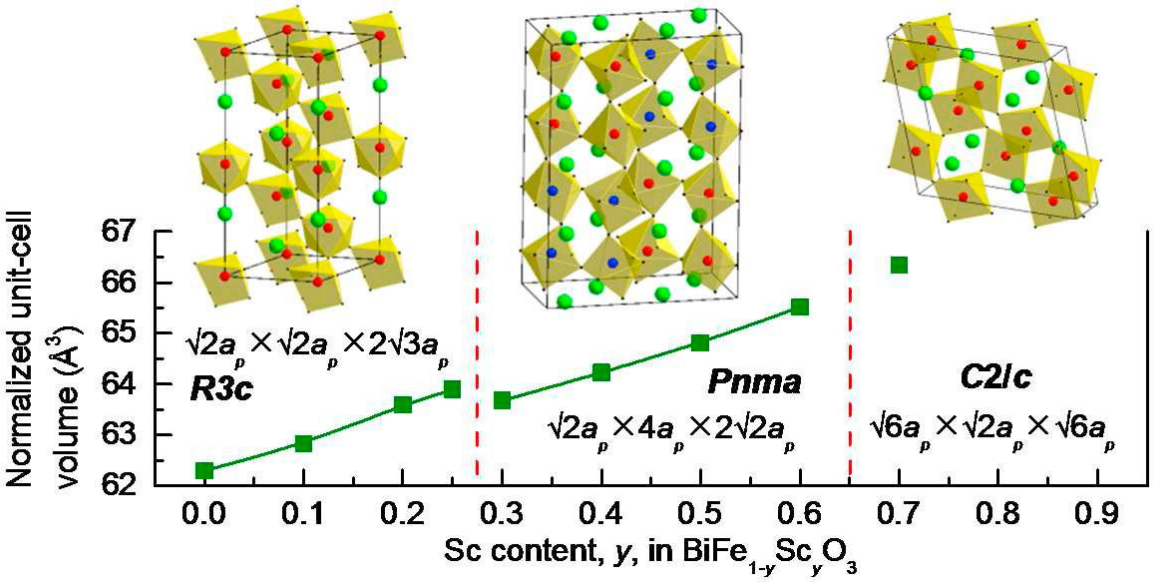

KEYWORDS: metastable phase, high-pressure synthesis, perovskite, sillenite

1. Introduction

Rhombohedral perovskite bismuth ferrite, $BiFeO_3$, combines all three ferroic orders in one structural phase [1,2]. A polar order results from parallel off-centre displacements of Bi^{3+} cations, a magnetic order is induced by exchange interactions between Fe^{3+} cations in oxygen octahedra, and an elastic order originates from correlated rotations (tilts) of these octahedra. Besides, bismuth ferrite is one of very few *type-I* perovskite multiferroics that can be produced using the conventional preparation methods, particularly the ceramic technique [2,3]. However, in spite of the availability and importance of bismuth ferrite for studies of the multiferroic phenomena, this compound can hardly be used in practice. Because of modulation of the spin structure, the macroscopic magnetization of $BiFeO_3$ is averaged to zero [4]. Furthermore, the Curie temperature and the Neel temperature of bismuth ferrite are too high (1083 K and 643 K, respectively [2]), which makes ineffective an exploitation of the lattice-magnetic coupling effect in the operating range of the majority of electronic devices. Pure $BiFeO_3$ is difficult to prepare since numerous parasitic phases form in the Bi_2O_3-Fe_2O_3 system at near the same conditions as the perovskite phase does [3]. A problem of stabilization of perovskite phase as well as an adjustment of physical properties are usually solved by means of modification of chemical composition. Indeed, using the conventional preparation methods, the perovskite

solid solutions with gradual substitution of Bi^{3+} by a trivalent cation (as a rule, a rare-earth one) were successfully obtained. At the relatively small substitution rates (typically, below 10-15 at.%), the crystal structure remained rhombohedral described by the *R*3*c* space group as that of the parent compound. An increase of the substitution rate results in formation of other perovskite phases (Ref [5] and references therein). In most cases, these phases coexist over wide compositional ranges. Through the Bi-site substitutions, the polar order and the tilting configuration of oxygen octahedra were modified, while the magnetic ordering temperature remained basically the same as that in $BiFeO_3$. Wide-range substitutions in the Fe site using the conventional methods were not very successful. In case of cations with either higher oxidation state (Ta^{5+}, Ti^{4+}) [6,7] or lower oxidation state (Mg^{2+}) [8] than that of Fe^{3+}, the substitution rates of order of few at.% only were achieved. Although some physical properties (e.g., electrical resistivity) were improved, those substitutions have induced no change in the crystal structure symmetry. Even when the substituting cation was Mn^{3+}, which is very similar to Fe^{3+} in terms of size and electronic configuration, the maximal rate did not exceed about 30 at.% [9,10] and crystal structure symmetry of the obtained solid solutions remained the rhombohedral, *R*3*c*.

It is known that although most of Bi-containing compositions of both the $Bi\mathit{B}^{3+}O_3$-type and the $Bi\mathit{B}^{2+}_{0.5}\mathit{B}^{4+}_{0.5}O_3$-type do not crystallize in perovskite structure at ambient pressure, they can be obtained as metastable perovskite phase by means of quenching from 1000-1500 K under a pressure of 4-6 GPa (the high-pressure synthesis) [11-16]. It should be pointed out that the magnitude of the applied pressure does matter: in particular, a pressure of several tens of MPa was not enough to synthesize single-phase solid solutions of $BiFe_{0.5}\mathit{B}^{3+}_{0.5}O_3$, where B^{3+}=Cr, Mn, Sc, Y [17]. Using the high-pressure synthesis method, single-phase perovskite solid solutions derived from $BiFeO_3$, in which 50 and more at.% of iron was substituted either by the cations of transition metals (Mn^{3+} [10,18,19], Co^{3+} [20,21], Cr^{3+} [22]) with the ionic size similar to that of Fe^{3+} or by Ga^{3+} [23] whose size is by 8% smaller, have been produced. Structural phases different from the parent rhombohedral *R*3*c* have been obtained and thoroughly studied. In all the above-mentioned solid solutions, the normalized unit-cell volume was found to decrease with increase of rate of substitution of Fe^{3+} by those trivalent cations.

We have recently reported on a high-pressure synthesis of the perovskite solid solution with the $BiFe_{0.5}Sc_{0.5}O_3$ composition [24]. One should noticed that the ionic size of Sc^{3+} is by 24% bigger than that of Fe^{3+}. Structure of the as-prepared samples was found to be orthorhombic *Pnma* similar to that reported for the $BiFe_{1-x}Mn_xO_3$ solid solutions in the range of $0.15 \le x \le 0.40$ synthesized under high pressure [10]. Combination of the antipolar displacements

of bismuth and the ++-- oxygen octahedral tilting results in a $\sqrt{2}a_p \times 4a_p \times 2\sqrt{2}a_p$ superstructure ($a_p \sim 4$ Å is the pseudocubic unit-cell parameter) of the *Pnma* phase in $BiFe_{0.50}Sc_{0.50}O_3$ [24,25]. This antipolar phase exhibits a long-range *G* type of antiferromagnetic order with a weak ferromagnetic component below about 220 K. It was revealed that the heating to about 770 K followed by cooling down to room temperature results an irreversible crossover from the orthorhombic *Pnma* phase to the orthorhombic *Ima*2 one via the intermediate high-temperature rhombohedral *R*3*c* phase. The *Ima*2 polymorph of $BiFe_{0.5}Sc_{0.5}O_3$ demonstrates the same type of magnetic order below 220 K as that of its antipolar polymorph and complex polar structure which makes this phase one of rare examples of canted ferroelectrics [24]. One can expect new structural phases and other types of polymorphism in solid solutions of the $BiFe_{1-y}Sc_yO_3$ system with the Fe/Sc ratio different from 1:1.

In this paper, we report on study of mutual solubility in the quasibinary $(1-y)BiFeO_3$-$yBiScO_3$ system. Samples with the nominal composition of $0.10 \le y \le 0.70$ were thermally treated at ambient pressure and under high pressure. Crystal structure of the obtained phases was characterized using methods of x-ray and neutron powder diffraction. The revealed compositional sequence in the high-pressure prepared perovskite $BiFe_{1-y}Sc_yO_3$ phases is discussed in comparison with the respective sequence in the $BiFeO_3$-$BiMnO_3$ system.

2. Experimental

Bi_2O_3 (>99.9%), Fe_2O_3 (>99.5%) and Sc_2O_3 (99.99%) were used as starting reagents to prepare the compositions of the $BiFe_{1-y}Sc_yO_3$ series. The oxides were mixed in the stoichiometric ratio, ball-milled in ethanol, dried, and pressed into pellets. The pellets were heated in a closed alumina crucible at fixed temperature in the range of 1040-1220 K for 10 min to 2 h and then quenched down to room temperature.

Thermal treatments under high pressure were performed using an anvil press DO-138A with a press capacity of 6300 kN. Both the raw oxide mixtures and the product of their pre-synthesis at ambient pressure (as described above) were explored. The powders were pressed into pellets of 4.5 mm in diameter and about 4 mm height. In order to avoid penetration of graphite from the tubular heater to the sample a protective screen of molybdenum foil was used. The samples were synthesized/sintered at 6 GPa and 1170-1470 K. The high-pressure treatment time was between 9 and 1 min (depending on temperature).

In order to estimate the stability limits of the perovskite phases prepared under high pressure, the obtained ceramic samples were annealed at temperatures between 770 and 1120 K

with a 50 K step. The samples were put a furnace heated to the certain temperature and quenched in air after a 2-h dwell.

An x-ray diffraction (XRD) study of the powdered samples was performed using either a DRON-3 diffractometer (phase analysis) or a PANalytical X'Pert MPD PRO diffractometer (phase analysis and the crystal structure characterization) in Cu Kα radiation at room temperature.

Neutron powder diffraction data were collected at the ISIS pulsed neutron and muon facility of the Rutherford Appleton Laboratory (UK), on the WISH diffractometer located at the second target station [26]. The sample was loaded into a 3-mm cylindrical vanadium can and measured at room temperature.

Rietveld refinement of the crystal structure was performed using the FullProf program [27].

Microstructure of the fractured surface and local chemical composition of the high-pressure prepared ceramics before annealing and after each annealing step were studied by scanning electron microscopy (SEM, Hitachi S-4100) equipped with an energy dispersive spectroscopy (EDS) detector.

3. Results and Discussion

3.1. Phase formation in the $BiFe_{1-y}Sc_yO_3$ system under ambient pressure

At a first step of the study, the thermal treatment of all the $BiFe_{1-y}Sc_yO_3$ samples ($0.10 \leq y \leq 0.70$) was performed at the certain temperature, 1040 K, which is the optimal temperature for synthesis of polycrystalline $BiFeO_3$ from simple oxides [28]. The treatment duration was 10 min.

It was found from analysis of the XRD patterns that the products of the thermal treatment represented mixtures of two main phases with the ratio between them dependent on the relative content of scandium (Figure 1). Perovskite phase, which was present in the most amount in the sample of the $BiFe_{0.90}Sc_{0.10}O_3$ nominal composition, demonstrates the same rhombohedral distortion of the crystal lattice as that in the parent compound, $BiFeO_3$. However, the reflections are shifted to a lower angle range indicating a partial substitution of iron by scandium. Second phase was identified to be cubic, a sillenite-type, described by the *I*23 space group [29]. This structure type is derived from a γ-modification of Bi_2O_3, in which from 5 to 10 at.% of bismuth is in crystallographic position that is not equivalent to that of other bismuth and can be substituted by other elements, in particular, by iron and/or scandium [30-33].

Attempts were undertaken to change the phase ratio in favour of the perovskite phase. It turned out that double homogenization, increase of the reaction time, and variation of the

heating/cooling rates resulted in changes in neither quantitative ratio nor qualitative content of the observed phases. We managed to obtain a single-phase perovskite solid solution with y=0.10 when the treatment temperature was increased to 1140 K. However, the thermal treatment of the $BiFe_{1-y}Sc_yO_3$ samples with a higher scandium content at 1140, 1170 and 1220 K resulted in no desired effect: the relative amount of the perovskite phase in the product was almost the same as that in the material treated at 1040 K. Increase of the treatment temperature has resulted only in a transformation of the phase based on γ-Bi_2O_3 into the phase based on β-Bi_2O_3 with the tetragonal $\bar{}$ symmetry [30,34,35] The XRD patterns of a sample with y=0.50 treated at 1170 K and then at 1220 K is shown in Figure 2. It is seen that the sample treated at 1220 K followed by quenching consists of two phases, namely the rhombohedral perovskite phase and the tetragonal phase. An annealing of the sample at temperature below 1170 K led to a transition from the $\bar{}$ phase back to the I23 phase (Figure 2). The observed reversibility of the transformation indicates the same chemical composition of these phases.

3.2. Synthesis of the $BiFe_{1-y}Sc_yO_3$ perovskite phases under high pressure

High-pressure synthesis of the $BiFe_{1-y}Sc_yO_3$ ($0.20 \le y \le 0.70$) ceramics *directly* from the oxide mixture (without thermal treatment at ambient pressure) turned out to be unsuccessful: the product was not single-phase. XRD pattern of the sample with the nominal composition of $BiFe_{0.60}Sc_{0.40}O_3$ prepared under high-pressure and high-temperature conditions from the as-milled oxide mixture is shown in Figure 3. It is seen that along with the diffraction reflections of the orthorhombic *Pnma* perovskite phase [24], extra reflections are present. Experiments with variations in temperature and duration of the high-pressure treatment did not result in vanishing of these reflections but allowed to attribute them to the same second phase which is a monoclinic high-pressure polymorph of bismuth oxide (HP-Bi_2O_3) [36]. No traces of the HP-Bi_2O_3 phase were detected in the $BiFe_{0.6}Sc_{0.4}O_3$ ceramics prepared at 6 GPa and 1170 K (9 min) from the mixtures thermally treated under ambient pressure at 1140 K for 10 min (Figure 3). It was found from the subsequent experiments that an increase of the high-pressure synthesis temperature to 1370 K allows shortening the process time to 1 min. Single-phase perovskite ceramics of the $BiFe_{1-y}Sc_yO_3$ composition ($0.20 \le y \le 0.70$) were synthesized under high pressure at temperatures from 1370 to 1470 K (depending on y) from the thermally treated oxide mixtures.

XRD patterns of the perovskite $BiFe_{1-y}Sc_yO_3$ ceramics with different y are shown in Figure 4. Based on a visual inspection of the patterns two ranges of compositional transitions at room temperature were suggested, namely between y=0.25 and 0.30, and between y=0.60 and 0.70.

Three types of the XRD patterns different in terms of splitting of the fundamental reflections were observed: rhombohedral (similar to that of $BiFeO_3$) at $y \leq 0.25$, orthorhombic (similar to the antipolar polymorph of $BiFe_{0.50}Sc_{0.50}O_3$ [24]) at $0.30 \leq y \leq 0.60$, and monoclinic (similar to that of $BiScO_3$ [37]) at y=0.70. The crystal structure refinements were successful using the rhombohedral $R3c$ space group (with the $\sqrt{2}a_p \times \sqrt{2}a_p \times 2\sqrt{3}a_p$ superstructure), the orthorhombic $Pnma$ group ($\sqrt{2}a_p \times 4a_p \times 2\sqrt{2}a_p$), and the monoclinic $C2/c$ group ($\sqrt{6}a_p \times \sqrt{2}a_p \times \sqrt{6}a_p$), respectively (see *Supporting Information*). The structural parameters obtained from the refinements are listed in Table 1.

Figure 5 shows the compositional dependence of the normalized unit-cell volume (V_p) of the perovskite $BiFe_{1-y}Sc_yO_3$ phases. One can see that the volume drops at the crossover from the rhombohedral to the orthorhombic composition range, while extrapolation of the $V_p(y)$ dependence of the *Pnma* phase to the $C2/c$ range suggests no anomaly at the border between the orthorhombic and the monoclinic ranges.

In order to compare and analyse the structure distortions over the whole compositional range studied, the lattice parameters obtained from the refinements were recalculated into the primitive perovskite unit-cell parameters [39]. We used the following relations for the basis vectors of the distorted structures and the parent cubic cell: $\boldsymbol{a_h}=-\boldsymbol{a_p}+\boldsymbol{b_p}$, $\boldsymbol{b_h}=-\boldsymbol{b_p}+\boldsymbol{c_p}$, $\boldsymbol{c_h}=2\boldsymbol{a_p}+2\boldsymbol{b_p}+2\boldsymbol{c_p}$ (the $R3c$ space group), $\boldsymbol{a_o}=\boldsymbol{a_p}+\boldsymbol{c_p}$, $\boldsymbol{b_o}=4\boldsymbol{b_p}$, $\boldsymbol{c_o}=-2\boldsymbol{a_p}+2\boldsymbol{c_p}$ (the *Pnma* space group) and $\boldsymbol{a_m}=2\boldsymbol{a_p}+\boldsymbol{b_p}+\boldsymbol{c_p}$, $\boldsymbol{b_m}=\boldsymbol{b_p}-\boldsymbol{c_p}$, $\boldsymbol{c_m}=-2\boldsymbol{a_p}+\boldsymbol{b_p}+\boldsymbol{c_p}$ (the $C2/c$ space group). These imply that the metric relations of the pseudocubic unit cell are $a_p = b_p = c_p$, $\alpha_p = \beta_p = \gamma_p \neq 90^o$ in the rhombohedral range, $a_p = c_p \neq b_p$, $\alpha_p = \gamma_p = 90^o \neq \beta_p$ in the orthorhombic range, and $a_p = c_p \neq b_p$, $\alpha_p = \gamma_p \neq \beta_p$, $\alpha_p \neq 90^o$, $\beta_p \neq 90^o$ in the monoclinic range (Figure 6). A radical rearrangement of the unit cell is seen to occur at the compositional crossover between y=0.25 and 0.30, while at the crossover between y=0.60 and 0.70 the change is certainly evolutional. The normalized unit cell of the *Pnma* phase transforms into the cell of the $C2/c$ phase just through onset of a small deviation (~0.2°) from the perpendicular direction of the $\boldsymbol{b}$ axis against the (a,c) plane.

Table 1. Structural parameters of the $BiFe_{1-y}Sc_yO_3$ system obtained from refinements of the XRD data and the neutron diffraction (ND) data.

y	Space group	*a* (Å)	*b* (Å)	*c* (Å)	β (deg.)	*V* (Å^3)	Z	note
0[a]	*R*3*c*	5.5787(2)		13.8688(3)		373.802(17)	6	XRD
0.10	*R*3*c*	5.5927(3)		13.9154(8)		376.940(36)	6	XRD
0.20	*R*3*c*	5.6152(3)		13.9725(9)		381.538(42)	6	XRD
0.25	*R*3*c*	5.6227(2)		14.0043(7)		383.430(27)	6	XRD
0.30	*Pnma*	5.6703(4)	15.7952(7)	11.3739(5)		1018.689(28)	16	XRD
0.40	*Pnma*	5.6785(2) **5.6782(4)**	15.8602(4) **15.8612(8)**	11.4101(9) **11.4117(8)**		1027.618(44) **1027.780(11)**	16	XRD **ND**
0.50	*Pnma*	5.6941(3) **5.6950(3)**	15.9088(8) **15.9126(5)**	11.4473(6) **11.4512(5)**		1036.979(33) **1034.672(78)**	16	XRD **ND**
0.60	*Pnma*	5.7265(8)	15.9265(6)	11.4936(7)		1048.269(22)	16	XRD
0.70	*C*2/*c*	9.8028(9)	5.7546(6)	9.9185(9)	108.341(6)	531.091(11)	8	XRD

[a]The data on $BiFeO_3$ (y=0) were taken from Ref. [38].

The same sequence of the structural phases has been observed in ceramics of the $BiFe_{1-x}Mn_xO_3$ system prepared under high-pressure: the rhombohedral *R*3*c* phase for x from 0 to about 0.10 is followed by the orthorhombic *Pnma* one which transforms into the monoclinic *C*2/*c* phase between x=0.60 and 0.80 [10,18]. It should be stressed here that, in contrast with the $V_p(y)$ dependence of the $BiFe_{1-y}Sc_yO_3$ perovskites (Figure 5), the normalized unit-cell volume in the $BiFe_{1-x}Mn_xO_3$ system *decreases* with increase of the Fe-substitution rate. In spite of this distinction in kind, in both these systems, V_p drops when crossing from the *R*3*c* range to the *Pnma* range. This is another evidence that crystal symmetry of Bi-based perovskites is determined mainly by the local atomic coordination of bismuth rather than geometrical criteria such as a tolerance-factor value [40,41]. Orthorhombic *Pnma* phase with the $\sqrt{2}a_p\times4a_p\times2\sqrt{2}a_p$ superstructure exist in wide ranges of the Fe-substitution in bismuth ferrite. Moreover, the same phase is observed in some $BiFeO_3$-based perovskites prepared at ambient pressure where bismuth is partly substituted by a rare earth cation [5,42,43]. However, no such phase has been detected in undoped $BiFeO_3$ although numbers of structural studies over wide ranges of either temperature or pressure have been undertaken. It seems that the *Pnma* ($\sqrt{2}a_p\times4a_p\times2\sqrt{2}a_p$) structural type requires more than one type of cation in at least one of the cation sites of a perovskite derived from $BiFeO_3$.

In order to estimate the limit of solubility of $BiScO_3$ in $BiFeO_3$ at ambient pressure, values of the average parameter ($a_{av}=V_p^{1/3}$) of the rhombohedral perovskite phase in all the

obtained $BiFe_{1-y}Sc_yO_3$ samples were calculated and compared. Figure 7 presents the a_{av} values as a function of scandium content for the *R*3*c* phase both in the high-pressure prepared ceramics and in the two-phase product obtained by means of the thermal treatment at ambient pressure as described in Part 3.1. Compositional dependence of lattice parameter of the second phase in the product, namely the cubic *I*23 one based on γ-Bi_2O_3, is shown in Figure 7 as well. Parameters of both phases prepared at ambient pressure grow with increase of the nominal scandium content that is agreement with a gradual substitution of iron by a larger cation. It should be noticed that although the growth become slower with increasing *y*, it does not saturate suggesting that the substitution continues over the whole compositional range studied. By extrapolation of the $a_{av}(y)$ dependence for the rhombohedral perovskite phase in the two-phase product until intersection with the respective dependence for the high-pressure prepared phase (Figure 7), the *maximal* scandium content in the $BiFe_{1-y}Sc_yO_3$ solid solution that can be obtained as a single phase at ambient pressure was estimated to be close to 0.15.

3.3. Stability of the high-pressure prepared $BiFe_{1-y}Sc_yO_3$ perovskites at ambient pressure

The perovskite ceramics prepared under high pressure were step-by-step annealed as indicated in *Experimental* followed by XRD analysis after each step. The annealing temperature was increased until reflections attributed to the cubic sillenite-type phase based on γ-Bi_2O_3 were detected in the XRD patterns. The thermal stability limit was defined as the temperature which is 50 K lower than that when the sillenite-type phase appears. The stability limit temperature of perovskite phase in the $BiFe_{1-y}Sc_yO_3$ system was found to depend on the scandium content and decreases as *y* increases (Table 2). Thus, the perovskite phases of the $BiFe_{1-y}Sc_yO_3$ composition ($0.20 \le y \le 0.70$) prepared under high pressure are metastable regardless of their crystal symmetry.

Table 2. Temperatures of the thermal stability limit of the perovskite phases in the $BiFe_{1-y}Sc_yO_3$ system.

Composition	Temperature
$y<0.15$	stable until melting
$0.20 \le y \le 0.25$	970 K
$0.30 \le y < 0.50$	920 K
$0.50 \le y \le 0.70$	870 K

The phases remained in the high-pressure prepared samples after annealing at temperatures by 100 K above their stability limits were identified to be the rhombohedral perovskite phase and the cubic sillenite-type one (Figure 8). The perovskite/sillenite phase ratio in the annealed samples was found to be the same as that in the products of the respective nominal compositions thermally treated at ambient pressure as described in Part 3.1. Moreover, the crystal lattice parameters of the corresponding phases were equal. Thus, the phases appeared after annealing of the high-pressure prepared ceramics and the phases formed as a result of thermal treatment of the oxide mixtures the same nominal composition at ambient pressure are identical.

Typical SEM images of fractured surface of the high-pressure synthesized samples before and after annealing at temperature above the stability limit are shown in Figure 9. Irregular-shape grains with signs of melting were observed in the as-prepared ceramics. No correlation between the chemical composition and the average grain size of the $BiFe_{1-y}Sc_yO_3$ ceramics has been detected. Grains with a rectangular prism shape were observed in the SEM images of the annealed samples whose XRD patterns demonstrated considerable amounts of the phase based on γ-Bi_2O_3. Such a grain shape is in a good agreement with the cubic symmetry of this phase.

4. Conclusions

The maximal iron-to-scandium substitution rate in $BiFeO_3$ that can be achieved using the conventional solid-state synthesis at ambient pressure does not exceed about 15 at.%. Crystal structure symmetry of the obtained solid solution is the rhombohedral, *R*3*c*. Thermal treatment of the $BiFe_{1-y}Sc_yO_3$ oxide mixtures with a higher content of scandium ($0.20 \le y \le 0.70$) results in formation of two main phases, namely a $BiFeO_3$-like *R*3*c* phase and a cubic (*I*23) sillenite-type phase based on γ-Bi_2O_3.

Single-phase perovskite ceramics of the $BiFe_{1-y}Sc_yO_3$ composition ($0.20 \le y \le 0.70$) can be prepared under high pressure at temperatures from 1370 to 1470 K from the pre-synthesized (10 min at 1140 K at ambient pressure) stoichiometric oxide mixtures. At room temperature, the as-prepared phase in the compositional range of $y \le 0.25$ is the rhombohedral *R*3*c* (with the $\sqrt{2}a_p \times \sqrt{2}a_p \times 2\sqrt{3}a_p$ superstructure). The orthorhombic *Pnma* phase ($\sqrt{2}a_p \times 4a_p \times 2\sqrt{2}a_p$) is observed for $0.30 \le y \le 0.60$, while phase with the $y=0.70$ composition is the monoclinic *C*2/*c* ($\sqrt{6}a_p \times \sqrt{2}a_p \times \sqrt{6}a_p$).

The perovskite $BiFe_{1-y}Sc_yO_3$ phases ($0.20 \le y \le 0.70$) prepared under high pressure are metastable regardless of their crystal symmetry. Their stability limit temperature depends on

the scandium content and decreases as y increases: from 970 K for the y=0.20 to 870 K for y=0.70. Annealing of the high-pressure prepared samples at temperatures above their stability limits results in formation of the two-phase mixtures with the same ratio between the rhombohedral $BiFeO_3$-like phase and the cubic sillenite-type one as that in the oxide mixtures the same nominal composition thermally treated at ambient pressure.

Acknowledgement

This work was supported by project TUMOCS. This project has received funding from the European Union's Horizon 2020 research and innovation programme under the Marie Skłodowska-Curie grant agreement No 645660. Financial support of the Belarusian Republican Foundation for Fundamental Research (Project No T15VT-008) is gratefully acknowledged as well. The authors thank Mr. M. Starykevich for help with the SEM study.

Appendix A. Supporting information

Supplementary data associated with this article can be found in the online version at http://dx.doi.org/10.1016/j.jssc.*******

References

1. N. Ortega, A. Kumar, J.F. Scott, R.S. Katiyar, Multifunctional magnetoelectric materials for device applications, *J. Phys.: Condens. Matter* 27 (2015) 504002(23).
2. A.P. Pyatakov, A.K. Zvezdin, Magnetoelectric and multiferroic media, *Physics - Uspekhi* 55 (2012) 557-581.
3. G. Catalan, J.F. Scott, Physics and applications of bismuth ferrite, *Adv. Mater.* 21 (2009) 2463-2485.
4. I. Sosnowska, T.P. Neumaier, E. Steichele, Spiral magnetic ordering in bismuth ferrite, *J. Phys. C* 15 (1982) 4835-4846.
5. D.C. Arnold, Composition-driven structural phase transitions in rare-earth-doped $BiFeO_3$ ceramics: a review, *IEEE Trans. Ultrasonics. Ferroelectrics Freq. Control* 62 (2015) 62-82.
6. Y.K. Jun, S.B. Lee, M. Kim, S.H. Honga, J.W. Kim, K.H. Kim, Dielectric and magnetic properties in Ta-substituted $BiFeO_3$ ceramics, *J. Mater. Res*. 22 (2007) 3397-3403.
7. V.A. Khomchenko, J.A. Paixaõ, Ti doping-induced magnetic and morphological transformations in Sr- and Ca-substituted $BiFeO_3$, *J. Phys.: Condens. Matter* 28 (2016) 166004(6).

8. H. Wu, Y.B. Lin, J.J. Gong, F. Zhang, M. Zeng, M.H. Qin, Z. Zhang, Q. Ru, Z.W. Liu, X.S. Gao, J.M. Liu, Significant enhancements of dielectric and magnetic properties in $Bi(Fe_{1-x}Mg_x)O_{3-x/2}$ induced by oxygen vacancies, *J. Phys. D: Appl. Phys*. 46 (2013) 145001(5).

9. A. Ianculescu, F.P. Gheorghiu, P. Postolache, O. Oprea, L. Mitoseriu, The role of doping on the structural and functional properties of $BiFe_{1-x}Mn_xO_3$ magnetoelectric ceramics, *J. Alloys Compd*. 504 (2010) 420-426.

10. A.A. Belik, A.M. Abakumov, A.A. Tsirlin, J. Hadermann, J. Kim, G.V. Tendeloo, E. Takayama-Muromachi, Structure and magnetic properties of $BiFe_{0.75}Mn_{0.25}O_3$ perovskite prepared at ambient and high pressure, *Chem. Mater*. 23 (2011) 4505-4514.

11. Y. Inaguma, T. Katsumata, High pressure synthesis, lattice distortion, and dielectric properties of a perovskite $Bi(Ni_{1/2}Ti_{1/2})O_3$, *Ferroelectrics* 286 (2003) 111-117.

12. Y. Inaguma, A. Miyaguchi, T. Katsumata, Synthesis and lattice distortion of ferroelectric/antiferroelectric Bi(III)-containing perovskites, *Mater. Res. Soc. Symp. Proc.* 755 (2003) 471-476.

13. S. Niitaka, M. Azuma, M. Takano, E. Nishibori, M. Takata, M. Sakata, Crystal structure and dielectric and magnetic properties of $BiCrO_3$ as a ferroelectromagnet, *Solid State Ionics* 172 (2004) 557-559.

14. D.D. Khalyavin, A.N. Salak, N.P. Vyshatko, A.B. Lopes, N.M. Olekhnovich, A.V. Pushkarev, I.I. Maroz, Yu.V. Radyush, Crystal structure of metastable perovskite $Bi(Mg_{1/2}Ti_{1/2})O_3$: Bi-based structural analogue of antiferroelectric $PbZrO_3$, *Chem. Mater*. 18 (2006) 5104-5110.

15. M.R. Suchomel, A.M. Fogg, M. Allix, H. Niu, J.B. Claridge, M.J. Rosseinsky, Bi_2ZnTiO_6: a lead-free closed-shell polar perovskite with a calculated ionic polarization of 150 μC cm^{-2}, *Chem. Mater.* 18 (2006) 4987-4989.

16. A.A. Belik, Polar and nonpolar phases of $BiMO_3$: A review, *J. Solid State Chem.* 195 (2012) 32-40.

17. I.V. Lisnevskaya, T.G. Lupeiko, E.A. Bikyashev, Synthesis of multiferroics $BiFe_{0.5}B_{0.5}O_3$, *Russ. J. Inorg. Chem*. 60 (2015) 140-146.

18. M. Azuma, H. Kanda, A.A. Belik, Y. Shimakawa, M. Takano, Magnetic and structural properties of $BiFe_{1-x}Mn_xO_3$, *J. Magn. Magn. Mater*. 310 (2007) 1177-1179.

19. P. Mandal, A. Sundaresan, C.N.R. Rao, A. Iyo, P.M. Shirage, Y. Tanaka, Temperature-induced magnetization reversal in $BiFe_{0.5}Mn_{0.5}O_3$ synthesized at high pressure, *Phys. Rev. B* 82 (2010) 100416(4).

20. M. Azuma, S. Niitaka, N. Hayashi, K. Oka, M. Takano, H. Funakubo, Y. Shimakawa, Rhombohedral-tetragonal phase boundary with high Curie temperature in $(1-x)BiCoO_3$-$xBiFeO_3$ solid solution, *Jpn. J. Appl. Phys*. 47 (2008) 7579-7581.

21. K. Oka, T. Koyama, T. Ozaaki, S. Mori, Y. Shimakawa, M. Azuma, Polarization rotation in the monoclinic perovskite $BiCo_{1-x}Fe_xO_3$, *Angew. Chem. Int. Ed.* 51 (2012) 7977-7980.

22. M.R. Suchomel, C.I. Thomas, M. Allix, M.J. Rosseinsky, A.M. Fogg, M.F. Thomas, High pressure bulk synthesis and characterization of the predicted multiferroic $Bi(Fe_{1/2}Cr_{1/2})O_3$, *Appl. Phys. Lett*. 90 (2007) 112909(3).

23. A.A. Belik, D.A. Rusakov, T. Furubayashi, E. Takayama-Muromachi, $BiGaO_3$-based perovskites: a large family of polar materials, *Chem. Mater*. 24 (2012) 3056-3064.

24. D.D. Khalyavin, A.N. Salak, N.M. Olekhnovich, A.V. Pushkarev, Yu.V. Radyush, P. Manuel, I.P. Raevski, M.L. Zheludkevich, M.G.S. Ferreira, Polar and antipolar polymorphs of metastable perovskite $BiFe_{0.5}Sc_{0.5}O_3$, *Phys. Rev*. B 89 (2014) 174414(11).

25. S.A. Prosandeev, D.D. Khalyavin, I.P. Raevski, A.N. Salak, N.M. Olekhnovich, A.V. Pushkarev, Yu.V. Radyush, Complex antipolar $\sqrt{2}\times4\times2\sqrt{2}$ structure with *Pnma* symmetry in $BiFeO_3$ and $BiFe_{1/2}Sc_{1/2}O_3$: First-principles calculations, *Phys. Rev. B* 90 (2014) 054110(6).

26. L.C. Chapon, P. Manuel, P.G. Radaelli, C. Benson, L. Perrott, S. Ansell, N.J. Rhodes, D. Raspino, D. Duxbury, E. Spill, J. Norris, Wish: The new powder and single crystal magnetic diffractometer on the second target station, *Neutron News* 22 (2011) 22-25.

27. J. Rodriguez Carvajal, Recent advances in magnetic structure determination by neutron powder diffraction, *Physica B* 193 (1993) 55-69.

28. T. Rojac, A. Bencan, B. Malic, G. Tutuncu, J.L. Jones, J.E. Daniels, D. Damjanovic, $BiFeO_3$ ceramics: processing, electrical, and electromechanical properties, *J. Amer. Ceram. Soc*. 97 (2014) 1993-2011.

29. S.F. Radaev, V.I. Simonov, Yu.F. Kargin, Structural features of γ-phase Bi_2O_3 and its place in the sillenite family, *Acta Cryst. B* 48 (1992) 604-609.

30. H.A. Harwig, On the structure of bismuthsesquioxide: the *α, β, γ,* and δ-phase, *Z. Anorg. Allg. Chem*. 444 (1978) 151-166.

31. S.F. Radaev, L.A. Muradyan, V.I. Simonov, Atomic structure and crystal chemistry of sillenites: $Bi_{12}(Bi^{3+}_{0.50}Fe^{3+}_{0.50})O_{19.50}$ and $Bi_{12}(Bi^{3+}_{0.67}Zn^{2+}_{0.33})O_{19.33}$, *Acta Cryst*. *B* 47 (1991) 1-6.

32. N. Rangavittal, T.N. Guru Row, C.N.R. Rao, A study of cubic bismuth oxides of the type $Bi_{26-x}M_xO_{40-delta}$ (*M*=Ti, Mn, Fe, Co, Ni or Pb) related to gamma-Bi_2O_3, *Eur. J. Solid State Inorg. Chem*. 31 (1994) 409-422.

33. A. Ducke, E. Muench, M. Troemel, Institut fur Anorganische Chemie, Frankfurt, Germany, ICDD Grant-in-Aid, Reference No. 00-043-0200, 1992.

34. M. Troemel, U. Delicat, A. Ducke, E. Muench, Institut fur Anorganische Chemie, Frankfurt, Germany, ICDD Grant-in-Aid, Reference No. 00-042-0201, 1991.

35. A. Ducke, E. Muench, M. Troemel, Institut fur Anorganische Chemie, Frankfurt, Germany, ICDD Grant-in-Aid, Reference No. 00-043-0181, 1992.

36. S. Ghedia, T. Locherer, R. Dinnebier, D.L.V.K. Prasad, U. Wedig, M. Jansen, A. Senyshyn, High-pressure and high-temperature multianvil synthesis of metastable polymorphs of Bi_2O_3: Crystal structure and electronic properties, *Phys. Rev. B* 82 (2010) 024106(12).

37. A.A. Belik, S. Iikubo, K. Kodama, N. Igawa, S. Shamoto, M. Maie, T. Nagai, Y. Matsui, S.Yu. Stefanovich, B.I. Lazoryak, E. Takayama-Muromachi, $BiScO_3$: centrosymmetric $BiMnO_3$-type oxide, *J. Amer. Chem. Soc*. 128 (2006) 706-707.

38. F. Kubel, H. Schmid, Structure of a ferroelectric and ferroelastic monodomain crystal of the perovskite $BiFeO_3$, *Acta Cryst.* B 46 (1990) 698-702.

39. A.N. Salak, D.D. Khalyavin, P.Q. Mantas, A.M.R. Senos, V.M. Ferreira, Structure-dependent microwave dielectric properties of $(1-x)La(Mg_{1/2}Ti_{1/2})O_3–xLa_{2/3}TiO_3$ ceramics, *J. Appl. Phys*. 98 (2005) 034101(8).

40. A.N. Salak, V.M. Ferreira, Microwave dielectric properties of Bi-substituted $La(Mg_{1/2}Ti_{1/2})O_3$, *J. Eur. Ceram. Soc*. 27 (2007) 2887-2891.

41. A.N. Salak, V.M. Ferreira, J.L. Ribeiro, L.G. Vieira, R.C. Pullar, N.McN. Alford, Bismuth-induced dielectric relaxation in the $(1-x)La(Mg_{1/2}Ti_{1/2})O_3$ - $xBi(Mg_{1/2}Ti_{1/2})O_3$ perovskite system, *J. Appl. Phys*. 104 (2008) 014105(10).

42. D.A. Rusakov, A.M. Abakumov, K. Yamaura, A.A. Belik, G. Van Tendeloo, E. Takayama-Muromachi, Structural evolution of the $BiFeO_3$-$LaFeO_3$ system, *Chem. Mater*. 23 (2011) 285-292.

43. D.V. Karpinsky, I.O. Troyanchuk, V. Sikolenko, V. Efimov, E. Efimova, M. Willinger, A.N. Salak, A.L. Kholkin, Phase coexistence in $Bi_{1-x}Pr_xFeO_3$ ceramics, *J. Mater. Sci.* 49 (2014) 6937-6943.

Highlights

- Maximal Fe-to-Sc substitution rate in $BiFeO_3$ at ambient pressure is about 15 at.%
- $R3c \rightarrow Pnma \rightarrow C2/c$ phase sequence in high-pressure prepared $BiFe_{1-y}Sc_yO_3$ ceramics
- The perovskite $BiFe_{1-y}Sc_yO_3$ phases formed under high pressure are metastable

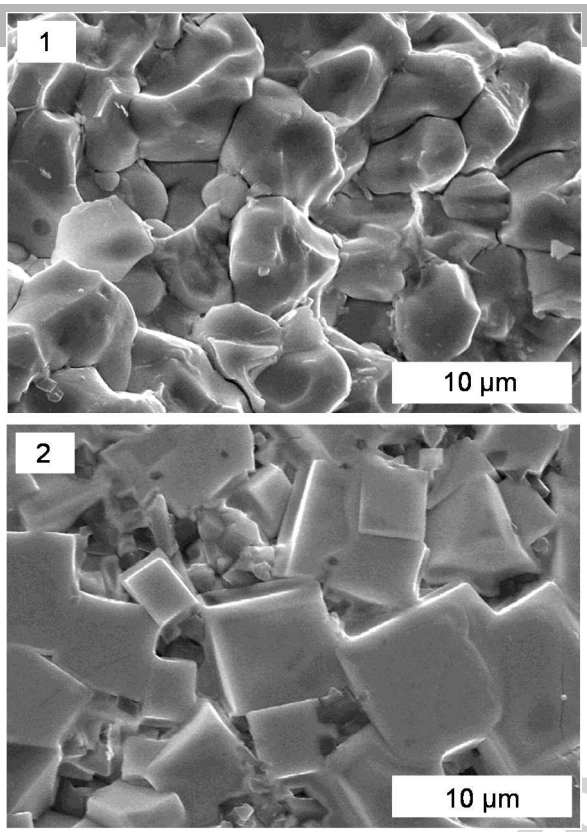

Figure 9. SEM images of the fractured surfaces of the $BiFe_{1-y}Sc_yO_3$ sample (y=0.45) thermally treated under high pressure: (1) as prepared and (2) annealed at 1070 K in air.

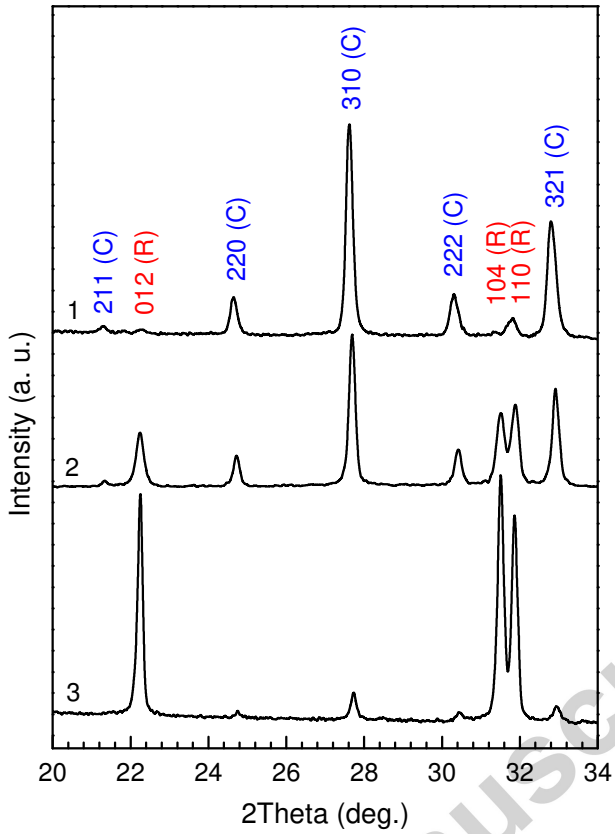

Figure 8. The XRD patterns of the $BiFe_{1-y}Sc_yO_3$ samples synthesized at 6 GPa and 1370-1470 K and then annealed in air at temperatures above the stability limits of their metastable perovskite phases: (1) the monoclinic *C*/2*c* in the sample with *y*=0.70, (2) the orthorhombic *Pnma* in the sample with *y*=0.45 and (3) the rhombohedral *R*3*c* in the samples with *y*=0.20. The diffraction reflections assigned to the rhombohedral (*R*3*c*) perovskite phase and to the cubic (*I*23) phase based on γ-Bi_2O_3 marked as (R) and (C), respectively.

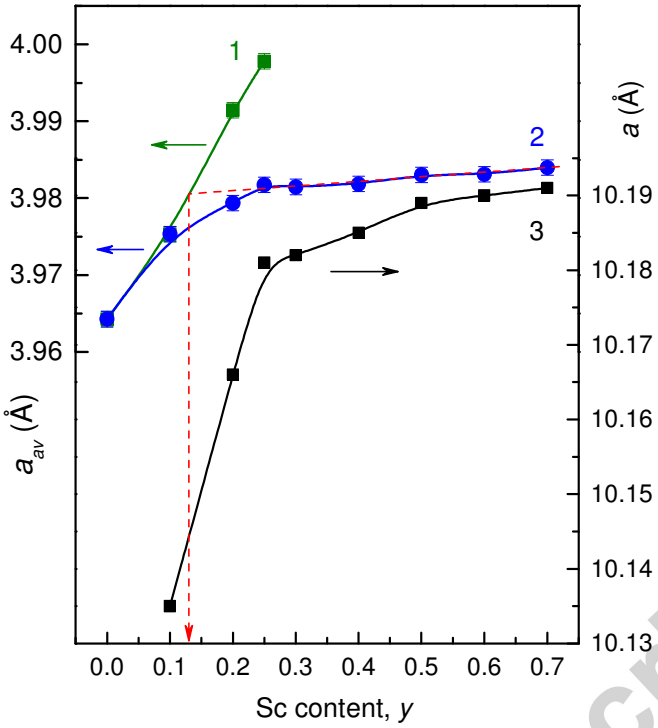

Figure 7. The average lattice parameters ($a_{av}=V_p^{1/3}$) of the rhombohedral $R3c$ perovskite phases prepared (1) under high pressure and (2) under ambient pressure, and (3) the lattice parameter of the cubic $I23$ phase based on γ-Bi_2O_3, as a function of scandium content, y.

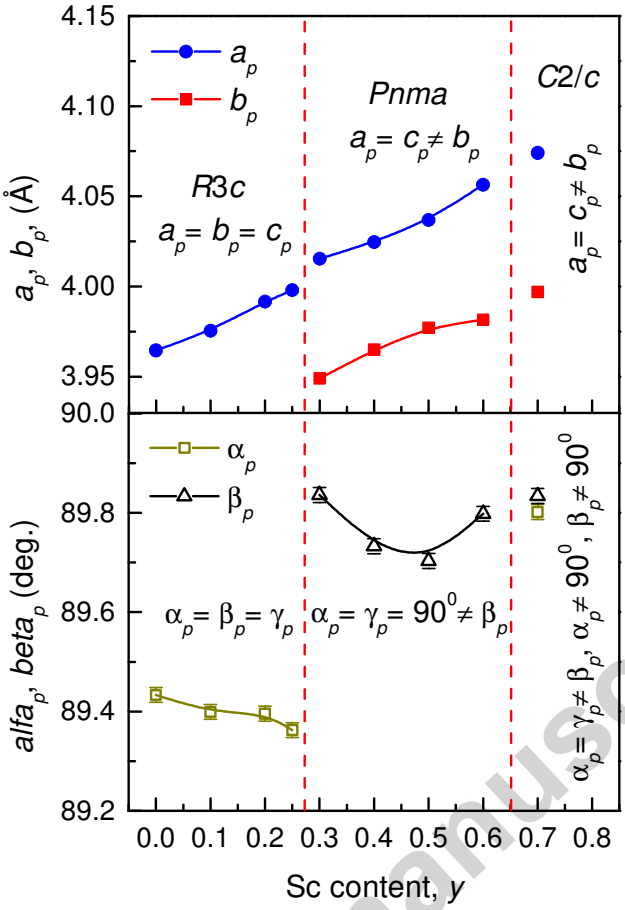

Figure 6. The primitive perovskite cell parameters of the $BiFe_{1-y}Sc_yO_3$ phases as a function of the scandium content, y, with the tentative borders of the different phase ranges. The space groups and the metric relations are indicated.

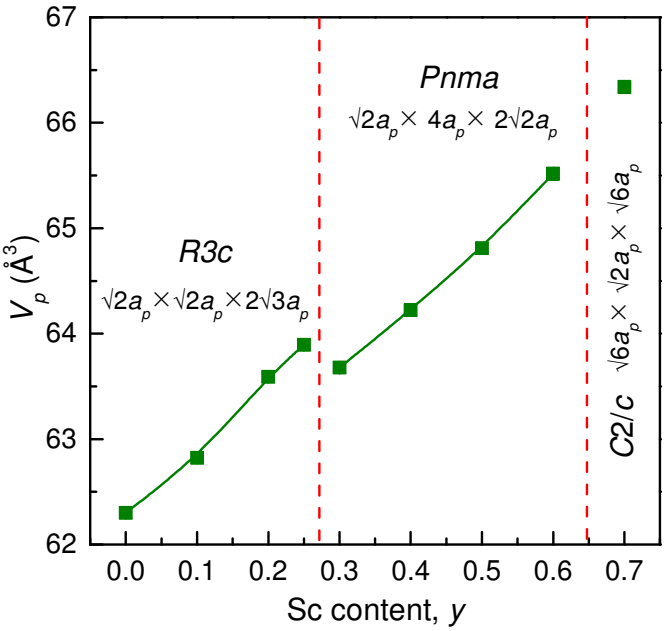

Figure 5. The normalized unit-cell volume of the $BiFe_{1-y}Sc_yO_3$ perovskite phases as a function of the scandium content, y, with the tentative borders of the different phase ranges. The space groups and the superstructures are indicated (a_p is the pseudocubic primitive perovskite unit-cell parameter).

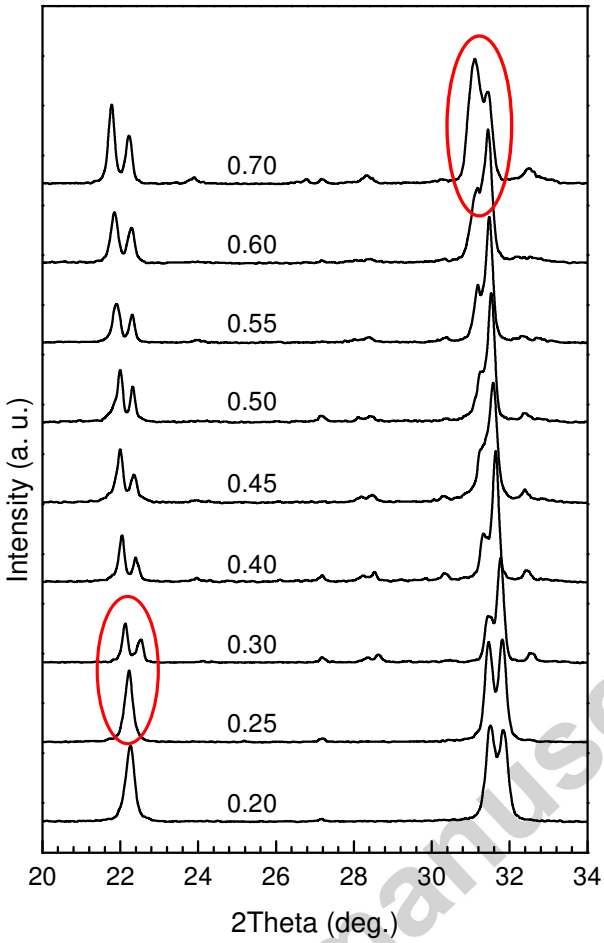

Figure 4. XRD patterns of the $BiFe_{1-y}Sc_yO_3$ samples ($0.20 \leq y \leq 0.70$) synthesized at 6 GPa and 1370-1470 K. The numbers denote the y values. The characteristic diffraction reflections indicative of the compositional phase transitions are highlighted.

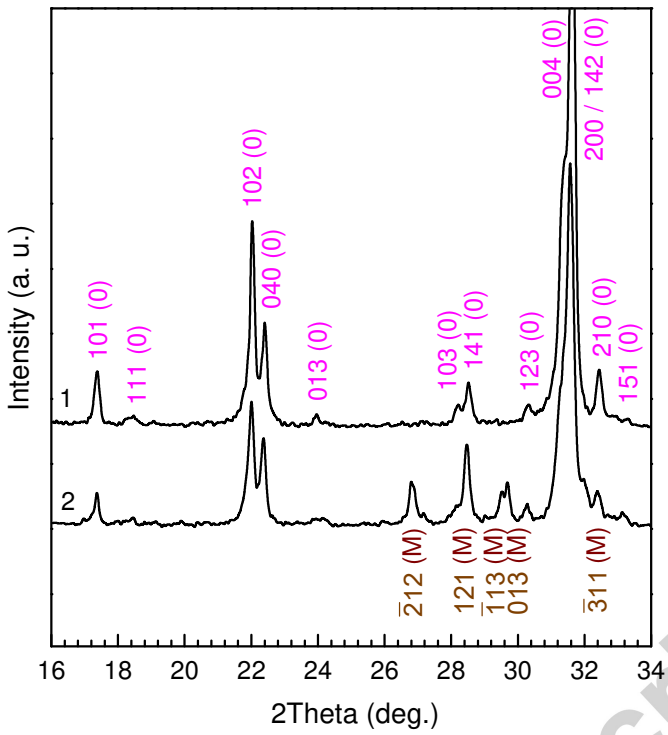

Figure 3. XRD patterns of the samples with the nominal composition of $BiFe_{0.60}Sc_{0.40}O_3$ synthesized at 6 GPa and 1170 K (9 min) either (1) from the mixture thermally treated at 1140 K for 10 min or (2) from the as-milled oxide mixture. The diffraction reflections assigned to the orthorhombic (*Pnma*) perovskite phase and to the monoclinic ($P2_1/c$) phase based on a high-pressure polymorph of Bi_2O_3 marked as (O) and (M), respectively.

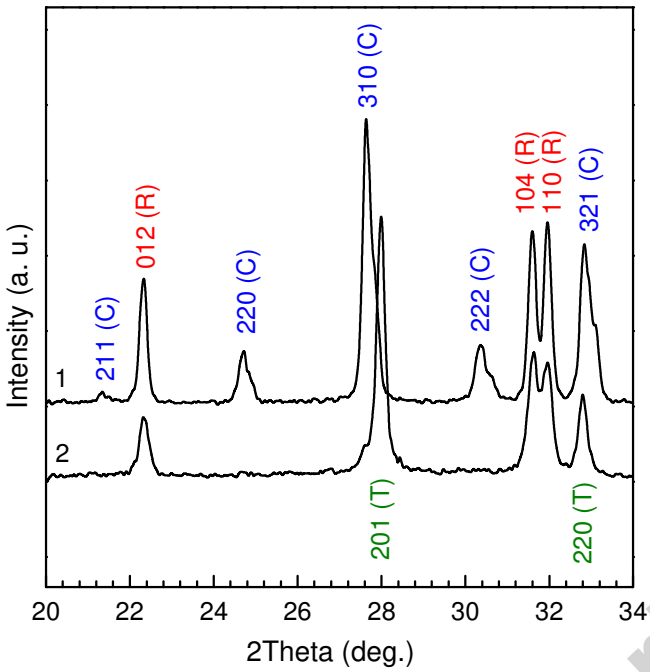

Figure 2. XRD patterns of the samples with the nominal composition of $BiFe_{0.50}Sc_{0.50}O_3$ thermally treated at 1140 K (10 min) and then at 1220 K (70 min) followed by either (1) annealing at 1070 with slow cooling to room temperature or (2) quenching. The diffraction reflections assigned to the rhombohedral (*R*3*c*) perovskite phase, to the cubic (*I*23) phase based on γ-Bi_2O_3, and to the tetragonal ($P\bar{4}2_1c$) phase based on β-Bi_2O_3, marked as (R), (C), and (T), respectively.

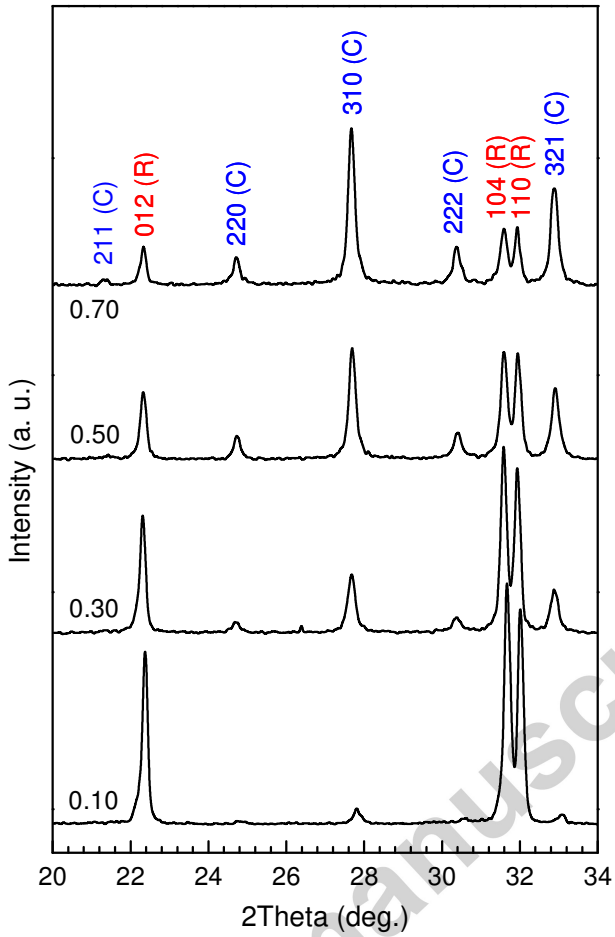

Figure 1. The most representative ranges of the XRD patterns of the $BiFe_{1-y}Sc_yO_3$ samples thermally treated under ambient pressure at 1040 K for 10 min. The numbers at each diffractogramme denote the *y* values. The diffraction reflections assigned to the rhombohedral (*R*3*c*) perovskite phase and to the cubic (*I*23) phase based on γ-Bi_2O_3 marked as (R) and (C), respectively.